Article

Patterning of phase-separated condensates by Dnd1 controls cell fate

Authors: Kim Joana Westerich[1], Katsiaryna Tarbashevich[1], Antra Gupta[1], Mingzhao Zhu[2], Kenneth Hull[2], Daniel Romo[2], Theresa Gross-Thebing[1†], Erez Raz[1*]

Affiliations

[1]Institute of Cell Biology, Center for Molecular Biology of Inflammation, University of Münster; 48149 Münster, Germany.

[2]Department of Chemistry & Biochemistry, Baylor University, Waco, Texas 76706, United States.

*Corresponding author. Email: erez.raz@uni-muenster.de

†Current address: Wellcome Trust/Cancer Research UK Gurdon Institute, Henry Wellcome Building of Cancer and Developmental Biology, Cambridge, UK.

SUMMARY

Germ granules, condensates of phase-separated RNA and protein, are essential for germline development, but how these molecules are organized within the granules and whether such an organization is relevant for germ cell fate is unclear. Combining three-dimensional *in vivo* structural and functional analyses, we study the dynamic spatial organization of molecules within zebrafish germ granules. We find that the vertebrate-specific Dead end protein is essential for positioning *nanos3* RNA at the condensates' periphery, where ribosomes are located. Without Dead end, or when translation is inhibited, *nanos3* RNA translocates into granule interiors, far from the ribosomes' location. These findings reveal the molecular mechanisms controlling the spatial organization of RNA within the phase-separated organelle and the importance of sub-granule RNA localization for preserving germ cell totipotency.

Key words

Zebrafish, germ cells, Dead end, *nanos*, RNA translation, germ granules, phase separation

INTRODUCTION

Germline development relies on molecules that reside within germ granules, phase-separated, non-membrane-bound condensates made of RNA and protein (RNP)[1–6]. However, the mechanisms that control the three-dimensional (3D) organization of the molecules within the condensates and the relevance of their organization for the function of the organelle are not fully understood[3–5]. An attractive model for studying these processes in vertebrates are zebrafish germ granules, given their relatively large size and accessibility for *in vivo* imaging[7]. A key component localized to these organelles is Dead end (Dnd1), a conserved RNA-binding protein that is essential for germline development in vertebrates. Loss of the protein results in sterility and the formation of germ cell tumors[8–13] and accordingly recent work showed that germ cells with impaired Dnd1 function fail to maintain their totipotency and acquire somatic fates[14]. Despite Dnd1's central role in controlling the fate of the vertebrate germline, the precise molecular function of the protein in the context of the phase-separated structure within which it resides is unknown. Here, we reveal a role for Dnd1 in regulating the spatial distribution and function of *nanos* RNA within germ granules, thereby ensuring proper development of the germline.

RESULTS

Nanos3 preserves germ cell fate and its mRNA is enriched at the periphery of germ granules

A known target of Dnd1 is the mRNA that encodes for the germ granule-localized protein Nanos3, which is essential for germ cell development in different organisms[15–19]. Our recent finding that germ cells depleted of Dnd1 adopt somatic cell fates[14] prompted us to evaluate whether inhibiting Nanos3 could similarly affect the cells. To investigate this, we employed embryos carrying a mutation in the gene encoding for the chemokine Cxcl12a that prevents germ cells from migrating toward the gonad, such that they reside at ectopic positions throughout the embryo (Fig. 1A)[20]. Interestingly, while non-manipulated ectopic germ cells maintain their shape independent of the tissue in which they reside, germ cells with depleted Nanos3 protein adopt various somatic cell shapes (e.g. that of a muscle cell, (Fig. 1A,B)), consistent with the idea that Dnd1 and Nanos3 function in the same pathway required for maintaining germ cell fate[14].

As the Dnd1 protein was previously shown to reside within germ granules[21], we aimed to determine if the granules are spatially organized with respect to the distribution of molecules and if so, whether Dnd1 plays a role in controlling it. To this end, we focused on the distribution of *nanos3* mRNA with respect to Dnd1, as well as that of Tudor domain containing 7 (Tdrd7) – encoding RNA and the granule-resident protein Vasa[7,22,23]. Here, we took advantage of the fact that during early embryonic stages (up to 10 hours post fertilization (hpf)), germ granules can be relatively large (Fig. S1A), ranging at sizes between 5 μm³ and 100 μm³, thus allowing for high spatial resolution analyses. We found that the germline-expressed mRNAs that encode Nanos3 and Tdrd7 are both enriched within the condensates (Fig. 1C), occupying largely non-overlapping punctate sub-granule positions (Fig. 1C). In contrast, the germline-expressed protein Vasa is distributed in a non-punctate pattern throughout the granule, allowing us to employ it for determining the volume and shape of the organelle (Fig. 1C, Fig. S1B, Movie S1).

To further characterize the distribution of specific mRNAs and proteins within the phase-separated condensates *in vivo*, we developed a 3D signal-visualization approach that allowed us to determine the spatial organization of molecules within granules in the 5-100 mm³ range (Fig. S1B). Intriguingly, upon evaluating the distribution of *nanos3* and *tdrd7* along the center-to-periphery

axis of such germ granule condensates, we found that both mRNAs are more abundant in the peripheral layers, extending beyond the Vasa protein signal (Fig. 1D upper panels and Fig. 1E left graph, Movie S1). The bias in RNA distribution along this axis is observed in granules of different sizes, as evaluated by the ratio between the signal intensity at the periphery and core regions (Fig. 1F). The largely non-overlapping distribution pattern of the two RNA molecules (Fig. S1A, Movie S1) is similar to that observed in *Drosophila*, where distinct homotypic RNA clusters were found within germ granules[24–27]. Together, as exemplified by the analysis of *nanos3* and *tdrd7* RNAs, these findings demonstrate that zebrafish germ granules are patterned organelles that contain distinct homotypic RNA clusters, organized asymmetrically along concentric 3D layers.

Next, we set out to examine the localization of *nanos3* mRNA with respect to the Dnd1 protein, which was shown to interact with this transcript[28]. Indeed, both molecules exhibit a similar distribution within the granules, with elevated levels observed at the periphery of the condensate (Fig. 1D lower panels, 1e right graph), where clusters of the mRNA and protein are found adjacent to each other, partially overlapping (Fig. S1C, Fig. 2A,B). Interestingly, following the localization of these molecules in live embryos employing the PP7 RNA detection system[29,30], we found that Dnd1 protein and *nanos3* mRNA clusters are highly dynamic, but maintain their proximity over time (Fig. 2C, Movie S2). These findings highlight the fact that while the distribution of molecules within the granules can differ for different RNAs and proteins, the spatial relationships among them can be maintained. This suggests cross dependency in localization among molecules and functional significance for sub-granule organization.

Dnd1 is required to maintain *nanos3* mRNA clusters at the periphery of germ granule condensates

We have previously shown that *nanos3* mRNA is a target of Dnd1[28], that knocking down Dnd1 results in loss of germ cell pluripotency[14] and show here that knocking down Nanos3 results in a similar phenotype, where germ cells differentiate into somatic cells (Fig. 1A). These findings, together with the spatial relationships identified here between Dnd1 protein and *nanos3* RNA, prompted us to ask whether Dnd1 controls *nanos3* distribution within the granule. To investigate this, we examined the organization of germ granules in live embryos following inhibition of *dnd1* RNA translation (Fig. 2D,E). Although Dnd1 loss eventually leads to a decrease in germ granule size and number at later stages of development[14], we found that, at least until 10 hpf, the volume of large germ granules is not altered (Fig. S2A). Remarkably however, our 3D analysis of the distribution of molecules within the granules revealed a strong reduction in *nanos3* mRNA levels at the periphery of the condensate, concomitant with an increase in the mRNA level in the core (Fig. 2D,E left panels and graph). Consistent with findings showing that Dnd1 interacts with the 3'UTR of *nanos3* mRNA (*nos 3'UTR*)[28], we found that this region of the transcript is sufficient for Dnd1 to control localization of the RNA within the condensate (Fig. 2F,G). Critically, these results do not represent a global effect on RNA distribution, as the localization of *tdrd7* mRNA was not altered under these conditions (Fig. 2D,E right panels and graph). Thus, the distribution of different RNA molecules within germ granules can be regulated by distinct molecular mechanisms. Interestingly however, despite the dramatic effect of Dnd1 knockdown on the positioning of *nanos3* mRNA clusters within the granules, the discrete homotypic clustering of *tdrd7* and *nanos3* molecules was preserved (Fig. S2B). These findings show that the basis for segregating RNA species from one another differs from the mechanisms that control the spatial distribution of the clusters within the granule.

Zebrafish germ granule condensates are enriched with ribosomes at their periphery

The altered distribution of *nanos3* mRNA within the germ granule observed upon Dnd1 knockdown led us to examine whether the change in the spatial organization of the RNA could have a functional significance. As a first step in this analysis, we sought to determine the localization of factors that can regulate mRNA function. In line with recent findings in invertebrates suggesting that translationally silent mRNA molecules are stored within phases-separated granules[31,32], we found that the RNA-induced silencing complex (RISC) components *mir-430* and Argonaute protein 2 (Ago2) are enriched within zebrafish germ granules (Fig. 3A,B). Intriguingly, while the RISC-complex components are found throughout the germ granule, we find that the ribosomes are almost exclusively localized to the edge of the condensate (Fig. 3C, 60S ribosomal protein L10a staining). Ribosomes have also been observed at the periphery of *Drosophila* polar granules shortly after fertilization, but in this case they disappear from these sites prior to the formation of germ cell precursors[33]. The distinct L10a localization pattern observed in 10 hpf zebrafish embryos is also found at an earlier stage of germ cell development, shortly after specification of the germline and the initiation of maternal RNA translation (Fig. S3A)[34]. Importantly, the peripheral ribosome-rich regions partially overlap with the peripheral domains in which *nanos3* mRNA clusters reside (Fig. 4B,C). Interestingly, in addition to the peripheral enrichment of ribosomes, we detected intra-granule domains that lack Vasa signal, and instead ribosomes and overlapping *nanos3* mRNA are found (Fig. S3B). These observations suggest that the granule-resident Nanos3, a protein essential for germ cell development[17] (Fig. 1A), is translated primarily at the borders of the phase-separated material.

Dnd1 activity is essential for *nanos3* mRNA translation at the periphery of germ granule condensates

To gain further insight into the mechanisms by which Dnd1 controls the function of *nanos3* mRNA within germ granules, we next examined the effect of Dnd1 depletion on the translation of the RNA. Indeed, Dnd1-depleted germ cells show a strong reduction in Nanos3 protein levels, as evaluated by the translation of injected *nos 3'UTR*-containing RNA encoding for a GFP-Nanos3 fusion protein (Fig. 4A)[14]. Importantly, the strong reduction in Nanos3 protein synthesis was associated with a loss of the overlap between *nanos3* mRNA and the ribosomes at the germ granule periphery (Fig. 4B,C). This observation is consistent with the idea that Dnd1 aids in the association of the *nanos3* mRNA with ribosomes and, consequently, to mRNA translation, thereby facilitating Nanos3 protein production. To determine whether the translational status of the RNA *per se* could be instructive regarding the localization of *nanos3* mRNA, we inhibited translation initiation using a derivative of the natural product pateamine A, des-methyl, des-amino pateamine A (DMDAPatA)[35–37] (Fig. S4A). Focusing on germ granules, we observed a strong depletion of *nanos3* mRNA from the periphery of the granule following DMDAPatA treatment, with a concomitant increase in the level of the RNA in the core of the condensate (Fig. 4D,E). In addition to the effect of global inhibition of translation, specific inhibition of *nanos3* mRNA translation by mutating the first Kozak sequence-containing ATG led to a similar effect. Specifically, *egfp-nos 3'UTR* RNA, in which the translation start codon was mutated, accumulated in the center of the granule and was largely absent from the periphery (Fig. 4F,G). Importantly however, mutating all ATGs within the open reading frame eliminated the accumulation of the RNA within germ granules (Fig. S4B-D). This finding suggests that the stability and localization of *nanos3* mRNA

molecules to germ granules is controlled by interactions with translation initiation factors. Indeed, we found that translation initiation factors eIF4G, eIF4E and PolyA-binding protein (PABP) are enriched within the condensates, where they largely overlap with *nanos3* mRNA clusters (Fig. S4B,E).

Together, these findings are consistent with the idea that germ granules function as storage sites for mRNAs that are already associated with translation initiation complex proteins[38], whereby translation of these RNA molecules occurs specifically at the periphery of the condensate, where the ribosomes and translation initiation factors are detected.

Dnd depletion causes a translocation of *nanos3* mRNA to the condensate core rather than enhanced degradation at the periphery

Considering the effect of the translation status on *nanos3* mRNA localization as described above, we proceeded to investigate the mechanisms by which Dnd1 regulates the localization of *nanos3* mRNA to the granule periphery. Dnd1 was previously shown to interfere with the function of the micro-RNA (miRNA) *mir-430*, thereby increasing mRNA stability and translation[28]. Indeed, measuring the overall intensity levels of *nanos3* RNA, we found that the total amount of the mRNA is reduced within Dnd1-depleted germ cells at 10 hpf (Fig. 5A). Interestingly however, in contrast to the decrease in the overall mRNA levels within the cells, we observed a specific and strong elevation of the amount of *nanos3* mRNA within germ granules in the absence of Dnd1 (Fig. 5B). This increase in mRNA abundance suggests that a portion of the accumulated transcripts in the granule core is derived from the cytoplasm. More importantly, our findings indicate that the loss of transcripts from the periphery of the condensate (Fig. 2D) is a consequence of translocation to the core domain rather than merely representing a decay of mRNA at the granule periphery.

To further corroborate our hypothesis, we analyzed the effect of Dnd depletion in maternal zygotic (MZ) *dicer* mutants, which lack mature miRNAs[39,40] (Fig. 5C,D). Indeed, we found that *nanos3* mRNA localization to the condensate periphery was not restored in these mutants, indicating that the loss of *nanos3* mRNA from these sites is independent of miRNA activity. Rather, our findings suggest that the positioning of *nanos3* mRNA within the condensates is primarily controlled by its interaction with the active translation machinery. Together, we conclude that inhibition of Dnd1 renders *nanos3* mRNA inaccessible to the translation machinery, leading to its accumulation in the granule core, and consequently to a drop of Nanos3 protein levels.

DISCUSSION

Our findings reveal how phase-separated vertebrate germ granules are organized concerning the spatial distribution of RNAs, proteins and the translation machinery. Importantly, we found that following the formation and segregation of germ plasm into the future germ cells[6,41], patterning of the condensates is controlled by the vertebrate-specific RNA-binding protein Dead end, and we present the relevance of this arrangement for cell fate and germline development (Fig. 6).

For many organisms, post-transcriptional regulation and properties of phase separated condensates are key for specifying and preserving the fate of germ cells[42,43]. Indeed, recent studies have shown that translationally repressed mRNAs can accumulate in germ granules, where they are stored and protected from degradation[31,32]. At the same time, translation of such RNA molecules requires interactions between the transcripts and the translation machinery. In the case of early germ cell

development, RNA translation must occur rapidly to ensure the maintenance of germline fate and avoid trans-fating into cells of other lineages, yet sufficient RNA silencing must be sustained for translation at later stages. Generating and maintaining such sub-granule organization of molecules is especially challenging in vertebrate germ cells, where the volume of the condensates is exceptionally large (e.g., up to 6 µm in diameter in zebrafish vs. up to 500 nm in *Drosophila* in early germline development[44]).

Since we found that the ribosomes are located at the periphery of the phase-separated germ granules, the translation of RNAs, such as those encoding for Nanos, could be controlled by the degree of localization of the RNAs to the border of the granules. Our study shows that the vertebrate-specific protein Dnd1 plays a key role in controlling the accessibility of specific granule-localized RNA to the translation machinery, thereby ensuring the maintenance of the germline (Fig. 6). Similar to the effect of Dnd1 knockdown, inhibiting the translation caused *nanos* RNA to accumulate at internal locations of the granules, suggesting that the capability of the RNA to be translated is important for its localization. The mechanism we describe allows for the production of proteins required for germ cell specification and fate maintenance, which has to occur rapidly at this stage to avoid the trans-fating of germline cells.

While the precise mechanisms by which Dnd1 controls *nanos3* localization are unknown, our findings suggest that the formation of an active translation complex is required for maintaining mRNA clusters at the condensate periphery. Recent findings in *C. elegans* link P granule localization of *nanos* mRNA to translation repression[31,32]. Accordingly, association of repressors of *nanos3* translation in Dnd1-depleted germ cells could maintain the transcript at the core of the granule. Consistently, in *Xenopus,* Dnd1 was show to prevent association of translational repressor eIF3f with *nanos* mRNA[45]. It would be interesting to determine whether a similar mechanism functions in zebrafish as well.

Our findings thus suggest that while the function of Nanos is conserved across the animal kingdom, rapid localization and maintenance of the RNA to the periphery is more challenging in larger vertebrate germ granules. We provide evidence that Dnd1 is a key protein that ensures the proper localization and function of fate determinants such as *nanos* RNA. Consistently, we found that knocking down Nanos results in trans-fating of germ cells into somatic cells, a phenotype originally described for Dnd1[14].

ACKNOWLEDGMENTS

AUTHOR CONTRIBUTIONS

E.R. supervised the project. K.J.-W. and E.R. designed the work and wrote the manuscript. K.J.-W. performed all of the experiments except for the following: T.G.-T. quantified the cell shape of Nanos-depleted germ cells and A.G. acquired the respective microscopy images; K.T. generated MZ*dicer* mutants; M.Z. synthesized DMDAPatA, K.H. and D.R. supervised the synthesis of the
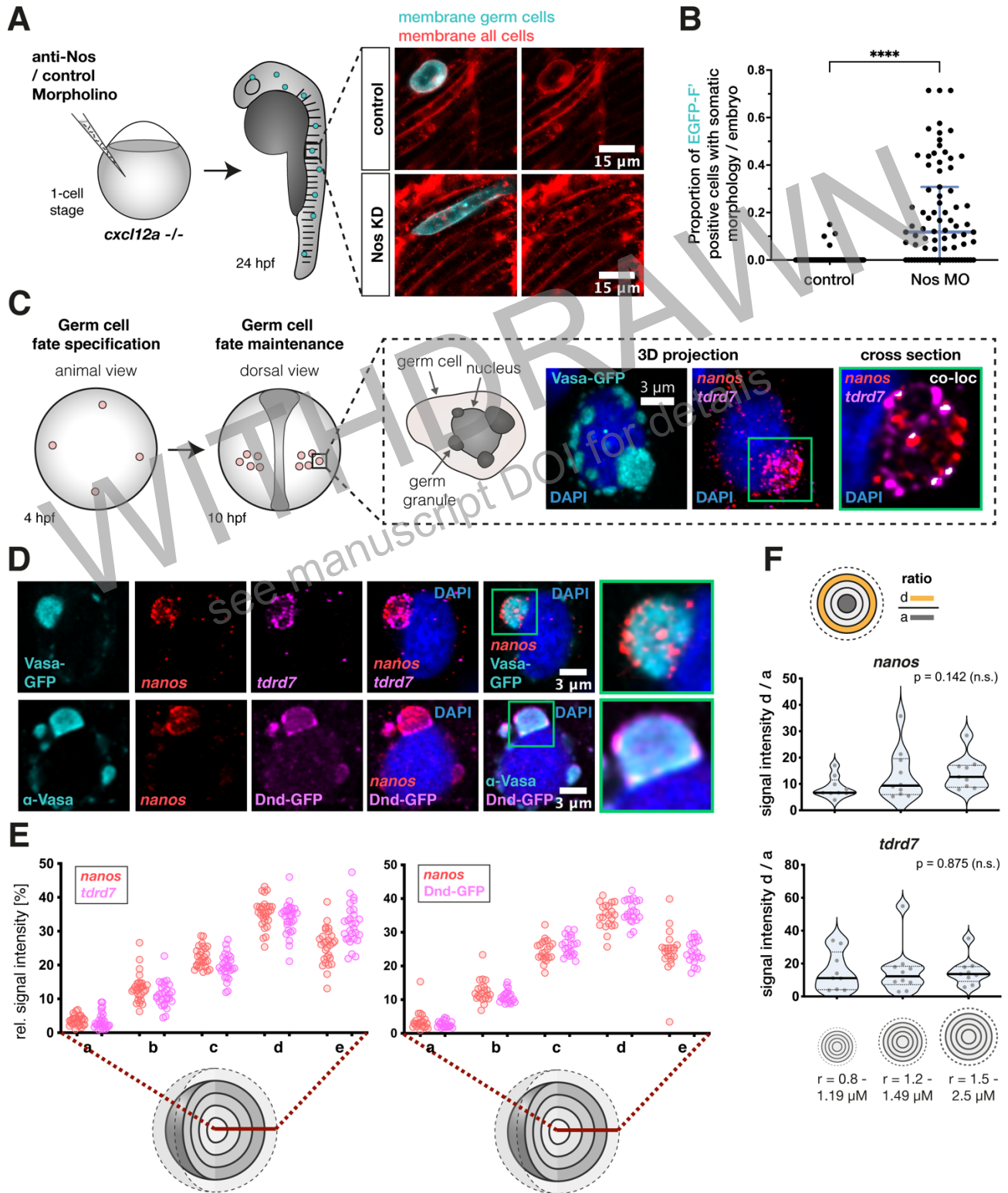
translation inhibitor, DMDAPatA. All authors read and approved the final manuscript with minor revisions.

DECLARATION OF INTERESTS

The authors declare that they have no competing interests.

FIGURES

Fig. 1. Nanos3 maintains germ cell fate, and its mRNA is localized to the periphery of germ granules

(A) 1-cell stage embryos that lack the chemokine guidance cue Cxcl12a were injected with a morpholino antisense oligonucleotide (anti-Nos Morpholino), inhibiting the translation of *nanos3* mRNA. The germ cells were then evaluated for somatic cell morphologies at 24 hpf. Images show an example of morphological transformation of Nanos3-deficient germ cells into elongated muscle precursor-like cells.

(B) Evaluation of the proportion of wildtype and Nanos3-deficient germ cells with somatic morphology per embryo.

(C) Scheme depicting early germ cell development. Germ cells are specified at 4 hpf, become migratory and form two bilateral clusters at 10 hpf. The black box shows a representative image of perinuclear germ granules marked by Vasa-GFP expression, with enrichment of endogenous germline mRNAs *tdrd7* and *nanos3* (detected by RNAscope probes).

(D) Distribution of *nanos3* mRNA relative to *tdrd7* mRNA (upper panels) and Dnd1 protein (lower panels) within germ granules marked by Vasa-GFP (upper panels) or immuno-stained Vasa protein (lower panels, α-Vasa).

(E) 3D analysis of the distribution of germ granule components along concentric layers of the condensate.

(F) 3D analysis of the ratio of mRNA abundance in the granule periphery (layer d) to that in the core (layer a) in large condensates that were categorized according to their size. r = radius. Significance was determined using Kruskal-Wallis test. n (r 0.8-1.19 µM) = 9, n (r 1.2-1.49 µM) = 10, n (r 1.5-2.5 µM) = 9. Number of experiments performed (N) = 3. n.s. = not significant.
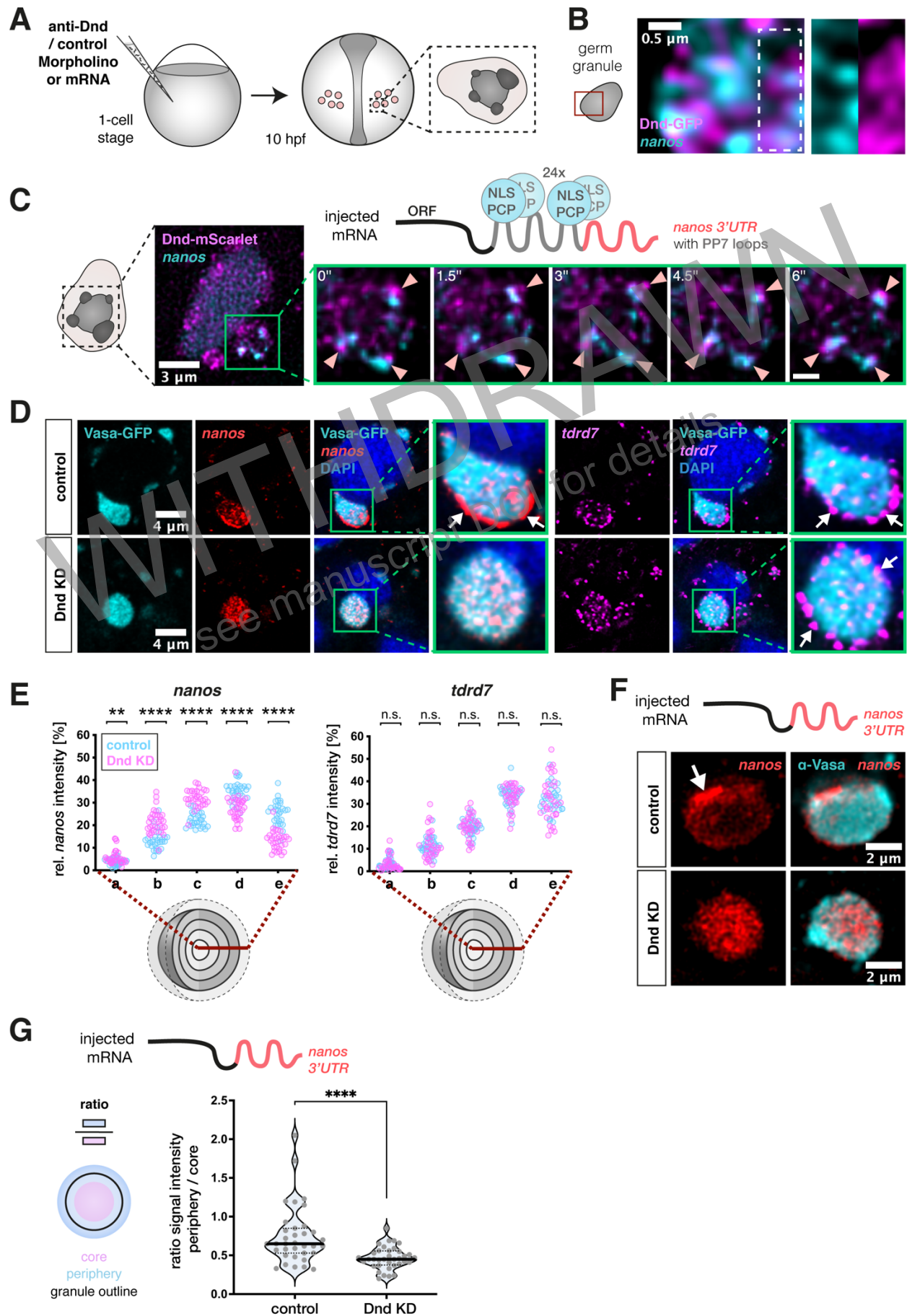
Fig. 2. Dnd1 is required for maintaining *nanos3* mRNA clusters at the periphery of germ granule condensates

(A) 1-cell stage embryos were injected with a morpholino antisense oligonucleotide inhibiting *dnd1* translation. Germ granules were analyzed at the 10 hpf stage.

(B) Localization of Dnd-GFP protein clusters and endogenous *nanos3* mRNA within the germ granule. White dotted box outlines region shown as a magnification in the right panels.

(C) The mobility of protein and mRNA clusters within germ granules was monitored in embryos injected with an mRNA containing the *nanos3* open reading frame (ORF) and PP7 stem loops inserted in the *nos 3'UTR*, along with mRNA encoding for the PP7 loop-detecting NLS-PCP-YFP coat protein and mRNA encoding for the Dnd-mScarlet protein. Green box shows a large germ granule with *nanos3* mRNA and Dnd1 protein clusters. Arrowheads in the magnification point to mRNA and protein clusters within this granule that remain in proximity over time. Time interval = 1.5 seconds, scale bar = 0.8 µm (see Movie S1).

(D) Distribution of endogenous *nanos3* and *tdrd7* mRNA within germ granules (marked by Vasa-GFP) in control and Dnd knockdown (KD) embryos. Green boxes show magnifications of large germ granule condensates from the image panels, with arrows pointing at mRNA enrichment at the granule periphery.

(E) 3D analysis of the distribution of endogenous *nanos3* and *tdrd7* mRNAs along germ granule concentric layers under control and Dnd KD conditions. Statistical significance was determined using Mann-Whitney U test. **P = 0.002, ****P< 0.0001. n (ctrl.) = 28, n (Dnd KD) = 32. N = 3.

(F and G) Localization of injected *nos 3'UTR*-containing mRNA within Vasa-stained germ granules under control and Dnd KD conditions. α = antibody. The graph shows the ratio of mRNA abundance in the granule periphery to that in the core of the condensate. Significance was determined using Mann-Whitney U test. ****P<0.0001. n (ctrl.) = 35, n (Dnd KD) = 36. N = 3.

11
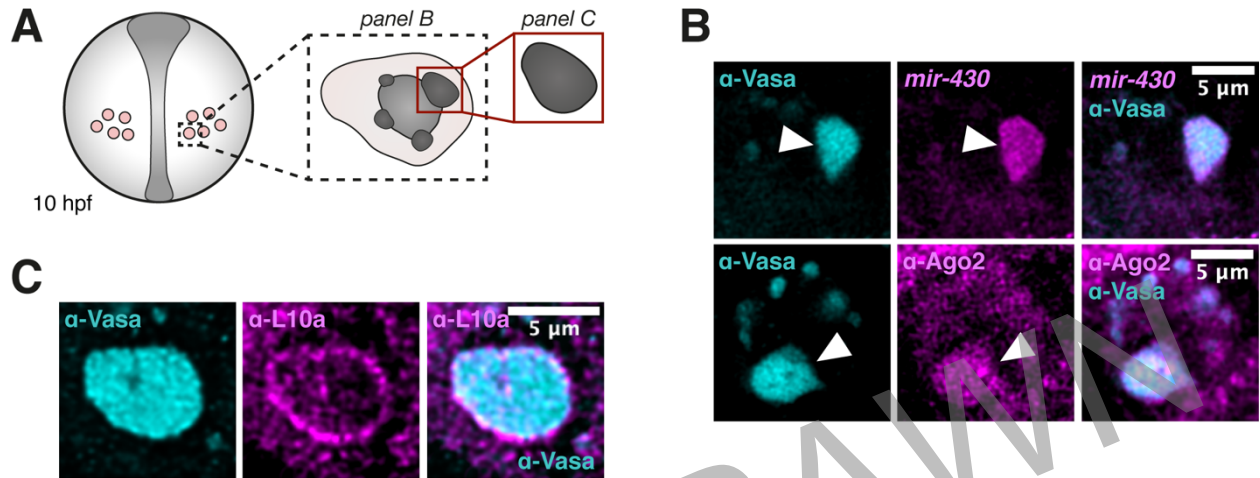
Fig. 3. Zebrafish germ granule condensates contain translation-repression factors and are enriched with ribosomes at their periphery

(A) A scheme showing germ cells in a 10 hpf embryo. Regulatory components were visualized within the cells, with panel B showing several granules within the cell and panel C focusing on a single large condensate.

(B) Co-visualization of Vasa protein and *mir-430* (detected by a miRCURY LNA miRNA probe) or Ago2 protein within germ cells. Arrowheads point at large germ granules. α = antibody.

(C) Co-detection of Vasa protein with 60S ribosomal protein L10a.
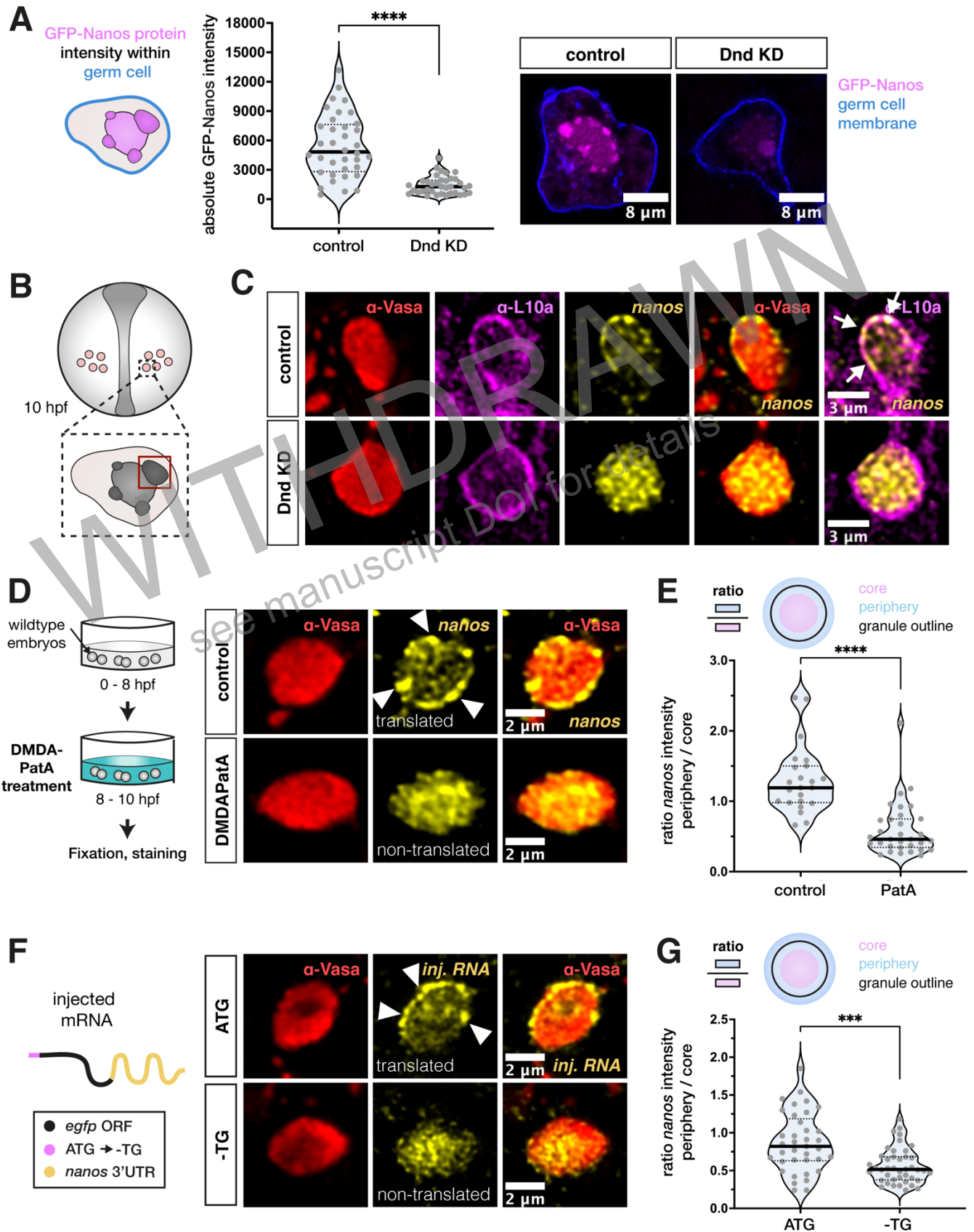
Fig. 4. Depletion of Dnd1 or inhibition of translation causes loss of *nanos3* mRNA from peripheral ribosome-rich areas of the germ granule
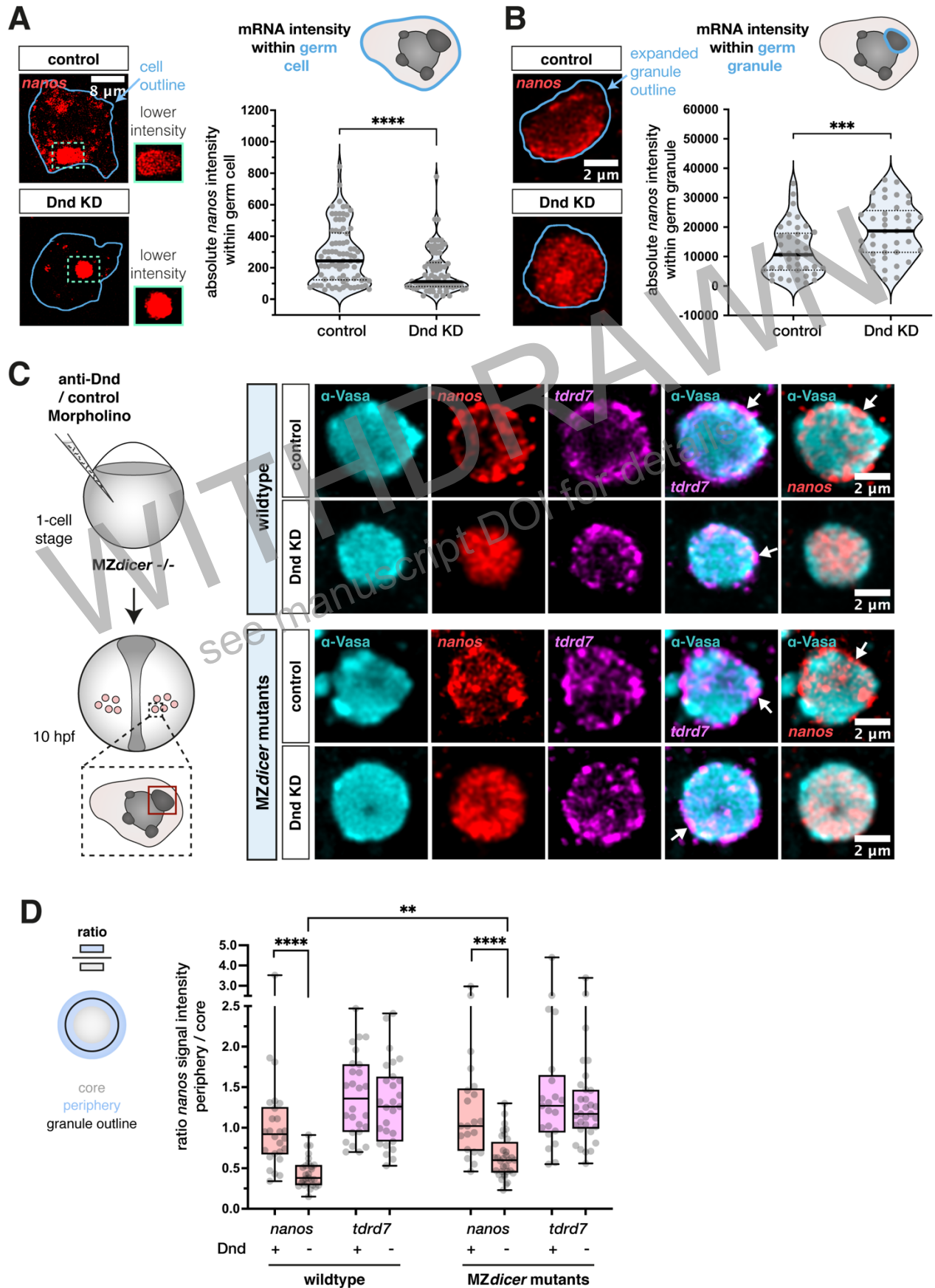
(A) Evaluation of the mean signal intensity of GFP-Nanos3 protein within germ cells under control and Dnd KD conditions. The blue cell outline in the scheme represents the border of the area of measurement. Significance was determined using Mann-Whitney U test. ****P<0.0001. n (ctrl.) = 36, n (Dnd KD) = 36. N = 3.

(B) A scheme depicting germ cells in a 10 hpf embryo. The red box outlines the region of interest within the germ cell (large condensate), which was considered for imaging and analysis.

(C) Visualization of endogenous *nanos3* mRNA localization with respect to Vasa and L10a proteins in germ granules under control or Dnd KD conditions. Arrows point to overlaps of L10a and *nanos3* at the condensate periphery. α = antibody.

(D, E) Localization of endogenous *nanos3* mRNA relative to Vasa protein in germ granules following control or DMDAPatA treatment. Arrowheads point at clusters of mRNA localized to the granule periphery. The graph shows the ratio of mRNA abundance between the granule periphery and the core of the condensate. Significance was determined using Mann-Whitney U test. ****P<0.0001. n (ctrl.) = 23, n (DMDAPatA) = 32. N = 3.

(F, G) Localization of injected *nos 3'UTR*-containing mRNA with respect to Vasa protein in germ granules. The first ATG of the open reading frame (ORF) is either functional (ATG) or mutated (-TG). The graph shows the ratio of mRNA abundance between the granule periphery and the core of the granule. Significance was evaluated using Mann-Whitney U test. ***P = 0.0002. n (ATG) = 52, n (-TG) = 46. N = 3.

Fig. 5. Loss of *nanos3* mRNA from the granule periphery in Dnd-depleted germ cells represents translocation to the condensate core that is independent of miRNA activity

(A) Analysis of the mean signal intensity level of endogenous *nanos3* mRNA within germ cells under control and Dnd KD conditions. The blue outline in the left panels marks the segmented cell outline, representing the area of measurement. Measurements were conducted across a 3D stack. Green dotted outlines show mRNA accumulation in a large condensate of the cell, and the green adjacent boxes show a magnification of the same area with a lower intensity value. Statistical significance was determined using Mann-Whitney *U* test. ****P<0.0001. n (ctrl.) = 82, n (Dnd KD) = 86. N = 3.

(B) Evaluation of the mean intensity of endogenous *nanos3* mRNA within large germ granules under control and Dnd KD conditions. Left image panels show mRNA accumulation along with a dilated outline of the segmented germ granule (light blue), which was considered as the area of measurement. Statistical significance was evaluated using Mann-Whitney *U* test. ***P = 0.0007. n (ctrl.) = 41, n (Dnd KD) = 41. N = 3.

(C, D) Localization of endogenous *nanos3* and *tdrd7* mRNA in wildtype (upper two rows of image panels) and MZ*dicer-/-* embryos (lower two rows of image panels) under control and Dnd KD conditions. The red box in the left scheme outlines a region of interest within the germ cell (large condensate), which was considered for imaging and analysis. Arrows in image panels point to mRNA enrichment at the condensate periphery. α = antibody. The graph shows the ratio between mRNA abundance in the granule periphery and the core. Significance was evaluated using Mann-Whitney *U* test. **P = 0.0021, ****P< 0.0001. Wildtype n (ctrl.) = 26, n (Dnd KD) = 27. MZ*dicer* n (ctrl.) = 21, n (Dnd KD) = 32. N = 3.

16
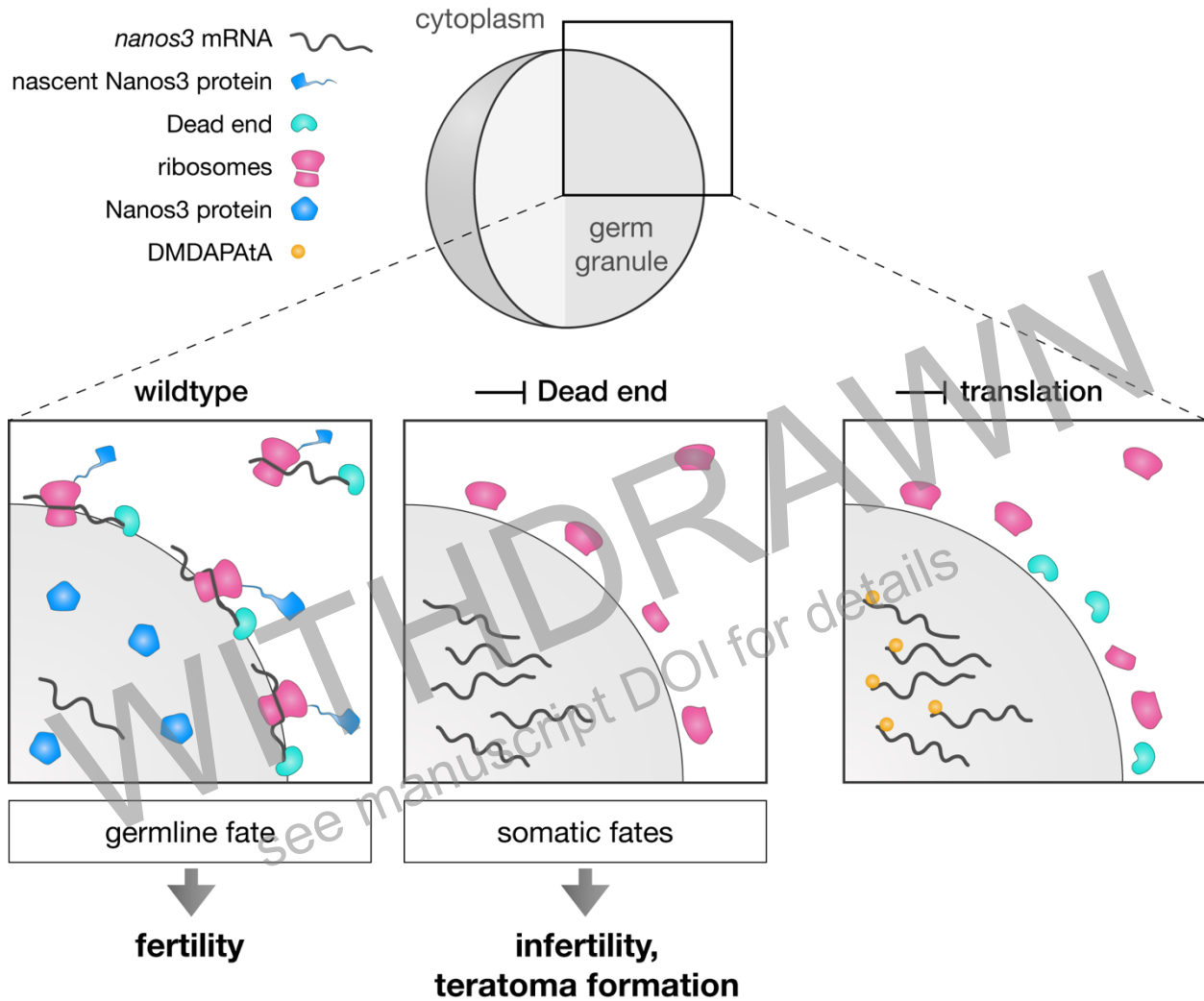
Fig. 6. Model of *nanos3* regulation by Dnd1 in phase-separated vertebrate condensates
In wildtype cells (left panel), *nanos3* mRNA associates with Dnd1 at the periphery of the germ granule, where ribosomes reside. At this site, an active translation complex forms on the mRNA, resulting in Nanos3 protein synthesis. Under these conditions, the germ cells maintain their fate, and a fertile organism develops. Upon depletion of Dnd1, *nanos3* mRNA translocates to the core of the condensate, where it is inaccessible to the ribosomes, resulting in lack of Nanos3 protein synthesis. As a result, the germ cells acquire somatic fates, leading to infertility. Upon inhibition of translation initiation complex assembly by DMDAPatA treatment (right panel), *nanos3* mRNA is not bound by ribosomes and translocates to the granule core.

METHODS

Resource availability

All source data are provided with this paper. Any information or requests for resources and reagents should be directed to the Lead Contact, Erez Raz (erez.raz@uni-muenster.de).

EXPERIMENTAL MODEL AND SUBJECT DETAILS

Zebrafish strains and handling

The following lines were used to obtain zebrafish (*Danio rerio*) embryos: wild type of the AB or AB/TL genetic background, *cxcr4b*[t26035] [46], *medusa*[NYO45] [47] and transgenic *kop-egfp-f-nos-3'UTR*[48]. Maternal zygotic (MZ) *dicer* embryos (*dicer*[hu715]) were generated by conducting a germline replacement as described previously[39]. Embryos were raised in 0.3× Danieau's solution (17.4 mM NaCl, 0.21 mM KCl, 0.12 mM MgSO$_4$·7H$_2$O, 0.18 mM Ca(NO$_3$)$_2$) at 25°C, 28°C or 31°C. The fish were handled according to the regulations of the state of North Rhine-Westphalia, supervised by the veterinarian office of the city of Muenster.

METHOD DETAILS

Cloning of DNA constructs

To follow mRNA using the PP7 detection system in live embryos, the sequence of 24 PP7 stem loops[49] was cloned into a Nanos3-nos 3'UTR plasmid[17] downstream of the open reading frame (ORF) sequence. The Dnd-mScarlet-nos 3'UTR plasmid was generated by replacing the GFP sequence of a Dnd-GFP-nos 3'UTR plasmid[50] with that of mScarlet. The *nos 3'UTR*-containing mRNAs used in Fig. 2F-G, Fig. 4F-G and Fig. S4B-C all carry an EGFP sequence in the ORF to allow for detection by RNAscope probes. For the generation of a non-translatable *nos 3'UTR*-containing mRNA used in Fig. 4 F-G, a 1-base pair deletion was introduced into the KOZAK-flanked ATG start codon of an EGFP coding sequence located upstream of the *nos 3'UTR* (EGFP^{-TG}-nos 3'UTR). For this purpose, site-specific mutagenesis was employed[51]. For the generation of a translatable *nos 3'UTR*-containing mRNA used in Fig. 2F-G and Fig. 4F-G, the sequence encoding for amino acids 2-15 was deleted from a full-length EGFP sequence-containing plasmid employing a Restriction free cloning approach[52] to prevent fluorescence emission of the EGFP protein (EGFP$^{Δ2-15}$-nos 3'UTR). This step was required to simultaneously visualize multiple RNA transcripts without emission of the EGFP protein. To generate a *nos 3'UTR*-containing mRNA lacking all start codons in the ORF used in Fig. S4B-C, all ATGs within the EGFP$^{Δ2-15}$-nos 3'UTR sequence were mutated to GTGs. Guanine was chosen to replace Adenine based on the structural similarity of the two bases. The respective ORF sequence carrying the ATG > GTG conversions was synthesized by Eurofins Genomics and cloned into a *nos 3'UTR*-containing plasmid. To generate the GFP-globin 3'UTR plasmid for global GFP expression in zebrafish, the GFP sequence was cloned upstream of a *Xenopus globin 3'UTR*.

Microinjection into zebrafish embryos

Capped sense mRNAs were synthesized using the mMessage mMachine kit (Ambion) according to the protocol of the manufacturer. 1 nL of mRNA and / or Morpholino-containing solution were injected into the yolk of 1-cell stage embryos. To mark the membrane of somatic cells, 45 ng/µl of *mcherry-f'-glob 3'UTR (A709)* were injected[53]. For visualization of protein within germ granules, *vasa-gfp-vasa 3'UTR* mRNA *(291)*[54] was injected at a concentration of 100 ng/µl, *dnd-gfp-nos 3'UTR (516)* mRNA[50] at 180 ng/µl and *mgfp-nanos-nos 3'UTR (356)* mRNA at 90 ng/µl [17]. For the evaluation of Dnd protein and *nanos3* mRNA movement, 140 ng of *nanos-nos 24xPP7*

3'UTR (D016) and 8 ng of *nls-ha-tdpcp-yfp-glob 3'UTR (C987)*[55] were co-injected with 100 ng of *dnd-mscarlet-nos 3'UTR (E513)*. To visualize *nos 3'UTR*-containing mRNA localization within germ granules, *egfp⁻ᵀᴳ-nos 3'UTR, egfpᐞ²⁻¹⁵-nos 3'UTR* and *egfpᐞ²⁻¹⁵_mut⁻ᴬᵀᴳ-nos 3'UTR (D366, E801, E845)* transcripts were injected at an equimolar concentration of 100 ng. For the evaluation of DMDAPatA drug efficiency, *gfp-globin 3'UTR* mRNA (B289) was injected at a concentration of 50 ng/µl. Nanos3 Morpholino (TGAATTGGAGAAGAGAAAAAGCCAT) was injected at a concentration of 60 µM[17], Dnd Morpholino (GCTGGGCATCCATGTCTCCGACCAT) at 20 µM or 30 µM (Fig. 4A)[50] and Cxcl12a MO (TTGAGATCCATGTTTGCAGTGTGAA) at 200 µM[20].

RNA detection and immunostaining of whole-mount embryos
For all treatments, embryos were fixed in 4% PFA overnight at 4°C (6 hpf and 10 hpf stage) or for 2 h at room temperature (RT, 10 hpf stage) under slow agitation. Embryos were subsequently rinsed in 1x PBT, dechorionated and transferred to and stored in 100% methanol. Detection of *mir-430* RNA in whole-mount embryos was performed using an in-situ hybridization procedure optimized for miRNA detection as previously described[56,57]. Dual labeled miRCURY LNA miRNA detection probes of *dre-mir-430a-3p* and *scramble-miR* (Qiagen, catalogue no. YD00613610-BCO and YD00699004-BCO) were hybridized at a concentration of 250 nmol overnight at 45°C. To co-visualize proteins with mRNAs within germ cells, an RNAscope *in situ* hybridization procedure was conducted using the RNAscope Multiplex Fluorescent Reagent Kit (ACD Bio) as previously described[58]. RNAscope probes Probe Diluent (ACD Bio 300041), Dr-nanos-C2 (ACD Bio 404521-C2), Dr-tdrd7-C2 (ACD Bio 536551-C2), EGFP-C1 (ACD Bio 400281-C1) and Dr-nanos3-CDS-C3 (ACD Bio 431191-C3) were hybridized overnight at 40°C. The embryos were then subjected to an immunostaining procedure as previously described, with a few modifications[58]. Briefly, embryos were permeabilized in 1x PBS containing 0.1% Tween-20 and 0.3% Triton X 100 (Carl Roth) for 1 h at RT and subsequently incubated in blocking solution (0.3% Triton X 100 and 4% BSA in 1x PBS) for 6 h at RT. Incubation with primary antibodies was then performed for 24 h at 4°C and incubation with secondary antibodies was done overnight at 4°C. The treatment with a GFP-targeting antibody was performed to enhance the fluorescent signal of expressed GFP-tagged Dnd protein. For the detection of Ago2 protein in germ cells, embryos were incubated in Dents solution (20% DMSO in methanol) for two days at 4°C, rehydrated in increasing amounts of 1x PBT in methanol (25%, 50%, 75% and 100%), re-fixed in 4% PFA for 20 minutes at RT and rinsed in 1x PBT. Embryos were then incubated in 1x PBT + 0.3% Triton X 100 for 1 h at RT and subsequently incubated for 5 h in blocking solution (1 x PBT + 20% goat serum + 5% DMSO) at RT. Subsequent treatment with primary and secondary antibodies was conducted as above.

Primary antibodies used: anti-Vasa (rabbit polyclonal, 1:400 dilution, GeneTex catalogue no. GTX128306), anti-GFP-1020 (polyclonal chicken, 1:600 dilution, Aves labs: SKU GFP-1020), anti-eIF4G (monoclonal mouse, 1:250 dilution, Sigma catalogue no. SAB1403762-100U), anti-PABP (polyclonal rabbit, 1:250 dilution, ThermoFisher catalogue no. PA5-17599), anti-eIF4E (polyclonal rabbit, 1:250 dilution, ThermoFisher catalogue no. PA5-86047), anti-L10a (monoclonal mouse, 1:100 dilution, Sigma catalogue no. WH0004736M1-100UG), anti-Ago2 (monoclonal mouse, 1:500 dilution, Abcam catalogue no. ab57113)

Secondary antibodies used: to visualize GFP, a 1:600 dilution of a 488 nm anti-chicken secondary antibody was employed (Jackson Immuno-Research); in all other cases, secondary antibodies from Thermo Fisher Scientific, catalogue no. A-11031, A-11034, A-11036 were employed using a 1:500 dilution for visualizing Vasa and a 1:1000 dilution for visualizing the remaining proteins.

Microscopy and image processing in zebrafish embryos
Images of germ granules in germ cells were acquired using a confocal microscope (LSM 710, Zeiss) equipped with 405 nm, 488 nm, 561 nm and 633 nm lasers and a 40x W N-Achroplan and a 63x W Plan-Apochromat objective (Zeiss). The ZEN software (Zeiss, version 2010B SP1, 6.0) was used to control the microscopy setup. Acquisition of different samples was conducted using the same pinhole size, optical slice thickness, gain and offset parameters. For images showing protein and RNA localization within germ granules, images were acquired with varying laser intensities (except for data presented in Fig. 4A and Fig. 5A-B) due to variability in germ cell depth within the organism and in germ granule size. This facilitated an optimal resolution without over exposure, which is required for accurately resolving mRNA structures. In this case, the mRNA signal intensities across the germ granule were expressed in relative amounts to compare the mRNA distribution among samples. For the 3D granule layer analysis in Fig. 1C-E and Fig. 2D-E, images of granules were acquired with a z-distance of 300 nm. To measure signal intensities of *nanos3* mRNA within germ cells (Fig. 5A), images were acquired with a z-distance of 1 μm. For the time lapse data shown in Fig. 2C and Movie S1, stacks with a z-distance of 500 nm were acquired with a Yokogawa CSU-X1 Spinning Disk microscope equipped with a Piezo-controlled 63x W Plan-Apochromat objective (Zeiss) and connected to a Hamamatsu Orca Flash 4.0 V3 camera. The VisiView software (Visitron, version 4.0.0.14) was used to control the setup of the microscope. For the verification of Pateamine A drug efficiency, data was acquired with a 5x EC Plan-Neofluar objective (Zeiss) on the Spinning Disk. Images were deconvolved using the Huygens Professional version 19.04 software (Scientific Volume Imaging, The Netherlands, http://svi.nl), employing the CMLE algorithm, with a maximum of 40 iterations.

DMDAPatA treatment of zebrafish embryos
To block translation of mRNAs, 8 hpf zebrafish embryos were incubated in Danieau's medium containing 10 μM DMDAPatA, a derivative of Pateamine A (synthesized by the lab of Daniel Romo, Baylor University) or DMSO for 2 h at 28°C. Embryos were then fixed in 4% PFA overnight at 4°C under slow agitation. Embryos were subsequently rinsed in 1x PBT, dechorionated and transferred to and stored in 100% methanol until subjected to RNAscope and immunostaining procedures. For the evaluation of drug efficiency, embryos were injected with 50 ng/μl of *gfp-globin 3'UTR* mRNA at the 1-cell stage and incubated with DMDAPatA or DMSO from the 16-cell stage until 5 hpf. Global expression of GFP was then compared between drug- and DMSO-treated embryos. Since DMDAPatA treatment stops embryonic development, the incubation period of these embryos was timed by monitoring the development of DMSO-treated control embryos, as described previously[59].

QUANTIFICATION AND STATISTICAL ANALYSIS

Evaluation of somatic cell shape acquisition by germ cells
To analyze the effect of Nanos3 depletion on the transfating potential of germ cells, *medusa^NYO45* embryos that lack expression of the guidance cue Cxcl12a were employed. In such embryos germ cells are localized at ectopic locations. Control or Nos Morpholino were injected at the 1-cell stage into these embryos, and the shape of germ cells was assessed at 24 hpf based on EGFP-F' expression. To have a clear definition of a somatic cell shape, germ cells were compared to three common somatic cell types (muscle, notochord or neuronal cells) and counted as acquiring a somatic cell shape only if their outline matched with either of these cell types. Subsequently, the

20

ratio between the number of germ cells with somatic cell shape and that with germ cell shape was calculated. For the images shown in Fig. 1A, Cxcl12a depletion was done by Morpholino injection.

3D layer analysis and volume measurement of germ granules

The analysis of mRNA and protein distribution within defined regions of the germ granule was conducted by employing a 3D image segmentation and processing workflow using the Software Imaris (Imaris 8.4.2, Oxford Instruments). The following steps were carried out to divide the germ granule volume into 3D layers (see also Fig. S1B): Germ granules imaged in the form of confocal stacks with a z-distance of 300 nm were pre-selected based on a minimum radius length of 750 nm and a clearly visible mRNA accumulation. A 3D segmentation of the granule was conducted based on an automated thresholding of the Vasa protein signal. Subsequently, the segmented granule was expanded or shrunk to several sizes using the 'Increase Surfaces' plugin (Imaris XTension, Dominic Filion). For this purpose, the ellipsoid minor axis length value was increased by 25% and then divided by five to obtain the value required for the plugin to generate five surfaces with an equal distance of the borders along the granule axis. Subtracting the masked molecule signal of each of the created surfaces created layers with equal thickness. Importantly, the outermost layer covers the space directly surrounding the granule, thus considering molecules that are associated with the outer granule surface. After evaluating the integrity of the layers, the mean molecule signal intensities were extracted for each layer and the share of signal relative to the total amount in the granule was calculated and presented in percentage. Finally, the germ granule size was determined by extracting the volume computed from the segmented Vasa protein signal. For the comparison of mRNA localization among different germ granule sizes, the ratio of the mean mRNA intensity in the peripheral layer to that in the core was determined. The dataset was divided into three subgroups according to the radius of the germ granules.

3D co-localization analysis among germ granule components

For the co-localization analysis of different germ granule components, the Coloc module of the software Imaris was used. To ensure an unbiased and reliable analysis, the following steps were implemented: a surface was created based on the signal of one of the two granule components (e.g., *nanos3* mRNA) and the automatically computed surface threshold value was extracted. The same process was repeated for the second granule component (e.g., *tdrd7* mRNA). The two extracted values were then multiplied by a factor of 1.7 (determined in pre-trials) and served as a minimum intensity threshold for co-localization. Values extracted from the co-localization analysis where the Pearson's Coefficient (PC) (graphs in Fig. S2B) and the amount of material co-localized above threshold (region of overlap in the graph in Fig. S1C).

Measurement of the periphery-core ratio of mRNA within germ granules

To quantify the relative distribution of mRNA in germ granules as shown in Fig. 2G, Fig. 4E,G and Fig. 5D, a ratio of the relative mRNA abundance between the periphery of the granule and the core region was determined. For this purpose, the following analysis was performed using the Fiji software (National Institutes of Health, version 2.0.0-rc-43/1.51a): A binary image of the Vasa granule marker channel was created using an auto intensity threshold, followed by a duplication of the image. One of the duplicated versions was dilated (3 iterations) to upscale the granule area, the other version is eroded (5 iterations) to downscale it. A region of interest (ROI) was defined around the dilated signal and inversed. This inversed ROI was combined with the ROI of the eroded signal. The combined ROI was inversed again, resulting in a layer-like space covering the periphery of the granule. Another ROI was created around the eroded signal to cover the core

21

region. Finally, using the two ROIs, the ratio of the mean mRNA intensity in the periphery to that in the core of the granule was determined.

Evaluation of absolute RNA and protein signal intensities within germ cells

RNA and protein signal intensity measurements shown in Fig. 4A, Fig. 5A,B and Fig. S4D were conducted with the Fiji software. For the measurement of mRNA intensities within germ granules, a cross section of a granule was segmented based on the Vasa protein signal as described above. The segmented granule outline was dilated with 3 iterations to upscale the granule area and thereby incorporate all peripheral mRNA signal. The dilated outline was used as a ROI to measure the mean intensity of the mRNA in this region. To measure mRNA intensities in the whole germ cell volume, cells were segmented across a 3D image stack of 1 µm-distanced slices based on a membrane marker signal that had been pre-processed with a median filter (2 x 10) for noise reduction. The resulting outlines were used as a ROI to extract the mean intensity of mRNA signal in the germ cell. Nanos3 protein levels within germ cells were measured employing the same approach, but focusing on a single cross section of the cell that covered the area of nucleus and germ granules.

Statistical analysis

The Prism software (version 9.4.0, Graphpad) was used to perform statistical analysis. Three biological replicates were conducted for each experiment, and the data pooled into one sample. Significance was evaluated using the Mann-Whitney *U* test for non-parametric data sets. Embryos and cells were analyzed with non-biased approaches.

References

1. So, C., Cheng, S., and Schuh, M. (2021). Phase Separation during Germline Development. Trends in Cell Biology *31*, 254–268. 10.1016/j.tcb.2020.12.004.

2. Dodson, A.E., and Kennedy, S. (2020). Phase Separation in Germ Cells and Development. Developmental Cell *55*, 4–17. 10.1016/j.devcel.2020.09.004.

3. Trcek, T., and Lehmann, R. (2019). Germ granules in Drosophila. Traffic *20*, 650–660. 10.1111/tra.12674.

4. Seydoux, G. (2018). The P Granules of C. elegans: A Genetic Model for the Study of RNA– Protein Condensates. Journal of Molecular Biology *430*, 4702–4710. 10.1016/j.jmb.2018.08.007.

5. Shin, Y., and Brangwynne, C.P. (2017). Liquid phase condensation in cell physiology and disease. Science *357*, eaaf4382. 10.1126/science.aaf4382.

6. Jamieson-Lucy, A., and Mullins, M.C. (2019). The vertebrate Balbiani body, germ plasm, and oocyte polarity. In Current Topics in Developmental Biology (Elsevier), pp. 1–34. 10.1016/bs.ctdb.2019.04.003.

7. Strasser, M.J., Mackenzie, N.C., Dumstrei, K., Nakkrasae, L.-I., Stebler, J., and Raz, E. (2008). Control over the morphology and segregation of Zebrafish germ cell granules during embryonic development. BMC Dev Biol *8*, 58. 10.1186/1471-213X-8-58.

8. Weidinger, G., Stebler, J., Slanchev, K., Dumstrei, K., Wise, C., Lovell-Badge, R., Thisse, C., Thisse, B., and Raz, E. (2003). dead end, a Novel Vertebrate Germ Plasm Component, Is

Required for Zebrafish Primordial Germ Cell Migration and Survival. Current Biology *13*, 1429–1434. 10.1016/S0960-9822(03)00537-2.

9. Slanchev, K., Stebler, J., de la Cueva-Méndez, G., and Raz, E. (2005). Development without germ cells: The role of the germ line in zebrafish sex differentiation. Proc. Natl. Acad. Sci. U.S.A. *102*, 4074–4079. 10.1073/pnas.0407475102.

10. Youngren, K.K., Coveney, D., Peng, X., Bhattacharya, C., Schmidt, L.S., Nickerson, M.L., Lamb, B.T., Deng, J.M., Behringer, R.R., Capel, B., et al. (2005). The Ter mutation in the dead end gene causes germ cell loss and testicular germ cell tumours. Nature *435*, 360–364. 10.1038/nature03595.

11. Horvay, K., Claußen, M., Katzer, M., Landgrebe, J., and Pieler, T. (2006). Xenopus Dead end mRNA is a localized maternal determinant that serves a conserved function in germ cell development. Developmental Biology *291*, 1–11. 10.1016/j.ydbio.2005.06.013.

12. Ruthig, V.A., Yokonishi, T., Friedersdorf, M.B., Batchvarova, S., Hardy, J., Garness, J.A., Keene, J.D., and Capel, B. (2021). A transgenic DND1GFP fusion allele reports in vivo expression and RNA-binding targets in undifferentiated mouse germ cells. Biology of Reproduction *104*, 861–874. 10.1093/biolre/ioaa233.

13. Gross-Thebing, T., and Raz, E. (2020). Dead end and Detour: The function of the RNA-binding protein Dnd in posttranscriptional regulation in the germline. In Current Topics in Developmental Biology (Elsevier), pp. 181–208. 10.1016/bs.ctdb.2019.12.003.

14. Gross-Thebing, T., Yigit, S., Pfeiffer, J., Reichman-Fried, M., Bandemer, J., Ruckert, C., Rathmer, C., Goudarzi, M., Stehling, M., Tarbashevich, K., et al. (2017). The Vertebrate Protein Dead End Maintains Primordial Germ Cell Fate by Inhibiting Somatic Differentiation. Developmental Cell *43*, 704-715.e5. 10.1016/j.devcel.2017.11.019.

15. Kobayashi, S., Yamada, M., Asaoka, M., and Kitamura, T. (1996). Essential role of the posterior morphogen nanos for germline development in Drosophila. Nature *380*, 708–711. 10.1038/380708a0.

16. Subramaniam, K., and Seydoux, G. (1999). nos-1 and nos-2, two genes related to Drosophila nanos, regulate primordial germ cell development and survival in Caenorhabditis elegans. Development *126*, 4861–4871. 10.1242/dev.126.21.4861.

17. Köprunner, M., Thisse, C., Thisse, B., and Raz, E. (2001). A zebrafish nanos-related gene is essential for the development of primordial germ cells. Genes Dev. *15*, 2877–2885. 10.1101/gad.212401.

18. Tsuda, M., Sasaoka, Y., Kiso, M., Abe, K., Haraguchi, S., Kobayashi, S., and Saga, Y. (2003). Conserved Role of nanos Proteins in Germ Cell Development. Science *301*, 1239–1241. 10.1126/science.1085222.

19. Julaton, V.T.A., and Reijo Pera, R.A. (2011). NANOS3 function in human germ cell development. Human Molecular Genetics *20*, 2238–2250. 10.1093/hmg/ddr114.

20. Doitsidou, M., Reichman-Fried, M., Stebler, J., Köprunner, M., Dörries, J., Meyer, D., Esguerra, C.V., Leung, T., and Raz, E. (2002). Guidance of Primordial Germ Cell Migration by the Chemokine SDF-1. Cell *111*, 647–659. 10.1016/S0092-8674(02)01135-2.

21. Slanchev, K., Stebler, J., de la Cueva-Méndez, G., and Raz, E. (2005). Development without germ cells: The role of the germ line in zebrafish sex differentiation. Proc. Natl. Acad. Sci. U.S.A. *102*, 4074–4079. 10.1073/pnas.0407475102.

22. Hay, B., Jan, L.Y., and Jan, Y.N. (1988). A protein component of Drosophila polar granules is encoded by vasa and has extensive sequence similarity to ATP-dependent helicases. Cell *55*, 577–587. 10.1016/0092-8674(88)90216-4.

23. Knaut, H., Pelegri, F., Bohmann, K., Schwarz, H., and Nüsslein-Volhard, C. (2000). Zebrafish vasa RNA but Not Its Protein Is a Component of the Germ Plasm and Segregates Asymmetrically before Germline Specification. Journal of Cell Biology *149*, 875–888. 10.1083/jcb.149.4.875.

24. Little, S.C., Sinsimer, K.S., Lee, J.J., Wieschaus, E.F., and Gavis, E.R. (2015). Independent and coordinate trafficking of single Drosophila germ plasm mRNAs. Nat Cell Biol *17*, 558–568. 10.1038/ncb3143.

25. Trcek, T., Grosch, M., York, A., Shroff, H., Lionnet, T., and Lehmann, R. (2015). Drosophila germ granules are structured and contain homotypic mRNA clusters. Nat Commun *6*, 7962. 10.1038/ncomms8962.

26. Niepielko, M.G., Eagle, W.V.I., and Gavis, E.R. (2018). Stochastic Seeding Coupled with mRNA Self-Recruitment Generates Heterogeneous Drosophila Germ Granules. Current Biology *28*, 1872-1881.e3. 10.1016/j.cub.2018.04.037.

27. Trcek, T., Douglas, T.E., Grosch, M., Yin, Y., Eagle, W.V.I., Gavis, E.R., Shroff, H., Rothenberg, E., and Lehmann, R. (2020). Sequence-Independent Self-Assembly of Germ Granule mRNAs into Homotypic Clusters. Molecular Cell *78*, 941-950.e12. 10.1016/j.molcel.2020.05.008.

28. Kedde, M., Strasser, M.J., Boldajipour, B., Vrielink, J.A.F.O., Slanchev, K., le Sage, C., Nagel, R., Voorhoeve, P.M., van Duijse, J., Ørom, U.A., et al. (2007). RNA-Binding Protein Dnd1 Inhibits MicroRNA Access to Target mRNA. Cell *131*, 1273–1286. 10.1016/j.cell.2007.11.034.

29. Bertrand, E., Chartrand, P., Schaefer, M., Shenoy, S.M., Singer, R.H., and Long, R.M. (1998). Localization of ASH1 mRNA Particles in Living Yeast. Molecular Cell *2*, 437–445. 10.1016/S1097-2765(00)80143-4.

30. Campbell, P.D., Chao, J.A., Singer, R.H., and Marlow, F.L. (2015). Dynamic visualization of transcription and RNA subcellular localization in zebrafish. Development, dev.118968. 10.1242/dev.118968.

31. Lee, C.-Y.S., Putnam, A., Lu, T., He, S., Ouyang, J.P.T., and Seydoux, G. (2020). Recruitment of mRNAs to P granules by condensation with intrinsically-disordered proteins. eLife *9*, e52896. 10.7554/eLife.52896.

32. Parker, D.M., Winkenbach, L.P., Boyson, S., Saxton, M.N., Daidone, C., Al-Mazaydeh, Z.A., Nishimura, M.T., Mueller, F., and Nishimura, E.O. (2020). mRNA localization is linked to translation regulation in the Caenorhabditis elegans germ lineage. Development, dev.186817. 10.1242/dev.186817.

33. Mahowald, A.P. (1971). Polar granules of Drosophila. IV. Cytochemical studies showing loss of RNA from polar granules during early stages of embryogenesis. J. Exp. Zool. *176*, 345–352. 10.1002/jez.1401760309.

34. Blaser, H., Eisenbeiss, S., Neumann, M., Reichman-Fried, M., Thisse, B., Thisse, C., and Raz, E. (2005). Transition from non-motile behaviour to directed migration during early PGC development in zebrafish. Journal of Cell Science *118*, 4027–4038. 10.1242/jcs.02522.

35. Romo, D., Choi, N.S., Li, S., Buchler, I., Shi, Z., and Liu, J.O. (2004). Evidence for Separate Binding and Scaffolding Domains in the Immunosuppressive and Antitumor Marine Natural Product, Pateamine A: Design, Synthesis, and Activity Studies Leading to a Potent Simplified Derivative. J. Am. Chem. Soc. *126*, 10582–10588. 10.1021/ja040065s.

36. Kuznetsov, G., Xu, Q., Rudolph-Owen, L., TenDyke, K., Liu, J., Towle, M., Zhao, N., Marsh, J., Agoulnik, S., Twine, N., et al. (2009). Potent in vitro and in vivo anticancer activities of des-methyl, des-amino pateamine A, a synthetic analogue of marine natural product pateamine A. Molecular Cancer Therapeutics *8*, 1250–1260. 10.1158/1535-7163.MCT-08-1026.

37. Kommaraju, S.S., Aulicino, J., Gobbooru, S., Li, J., Zhu, M., Romo, D., and Low, W.-K. (2020). Investigation of the mechanism of action of a potent pateamine A analog, des-methyl, des-amino pateamine A (DMDAPatA). Biochem. Cell Biol. *98*, 502–510. 10.1139/bcb-2019-0307.

38. Friday, A.J., and Keiper, B.D. (2015). Positive mRNA Translational Control in Germ Cells by Initiation Factor Selectivity. BioMed Research International *2015*, 1–11. 10.1155/2015/327963.

39. Giraldez, A.J., Cinalli, R.M., Glasner, M.E., Enright, A.J., Thomson, J.M., Baskerville, S., Hammond, S.M., Bartel, D.P., and Schier, A.F. (2005). MicroRNAs Regulate Brain Morphogenesis in Zebrafish. Science *308*, 833–838. 10.1126/science.1109020.

40. Bernstein, E., Kim, S.Y., Carmell, M.A., Murchison, E.P., Alcorn, H., Li, M.Z., Mills, A.A., Elledge, S.J., Anderson, K.V., and Hannon, G.J. (2003). Dicer is essential for mouse development. Nat Genet *35*, 215–217. 10.1038/ng1253.

41. Roovers, E.F., Kaaij, L.J.T., Redl, S., Bronkhorst, A.W., Wiebrands, K., de Jesus Domingues, A.M., Huang, H.-Y., Han, C.-T., Riemer, S., Dosch, R., et al. (2018). Tdrd6a Regulates the Aggregation of Buc into Functional Subcellular Compartments that Drive Germ Cell Specification. Developmental Cell *46*, 285-301.e9. 10.1016/j.devcel.2018.07.009.

42. Strome, S., and Updike, D. (2015). Specifying and protecting germ cell fate. Nat Rev Mol Cell Biol *16*, 406–416. 10.1038/nrm4009.

43. Bose, M., Lampe, M., Mahamid, J., and Ephrussi, A. (2022). Liquid-to-solid phase transition of oskar ribonucleoprotein granules is essential for their function in Drosophila embryonic development. Cell *185*, 1308-1324.e23. 10.1016/j.cell.2022.02.022.

44. Arkov, A.L., Wang, J.-Y.S., Ramos, A., and Lehmann, R. (2006). The role of Tudor domains in germline development and polar granule architecture. Development *133*, 4053–4062. 10.1242/dev.02572.

45. Aguero, T., Jin, Z., Chorghade, S., Kalsotra, A., King, M.L., and Yang, J. (2017). Maternal dead-end 1 promotes translation of nanos1 through binding the eIF3 complex. Development, dev.152611. 10.1242/dev.152611.

46. Knaut, H., Werz, C., Geisler, R., Nüsslein-Volhard, C., and The Tübingen 2000 Screen Consortium (2003). A zebrafish homologue of the chemokine receptor Cxcr4 is a germ-cell guidance receptor. Nature *421*, 279–282. 10.1038/nature01338.

47. Valentin, G., Haas, P., and Gilmour, D. (2007). The Chemokine SDF1a Coordinates Tissue Migration through the Spatially Restricted Activation of Cxcr7 and Cxcr4b. Current Biology *17*, 1026–1031. 10.1016/j.cub.2007.05.020.

48. Blaser, H., Eisenbeiss, S., Neumann, M., Reichman-Fried, M., Thisse, B., Thisse, C., and Raz, E. (2005). Transition from non-motile behaviour to directed migration during early PGC development in zebrafish. Journal of Cell Science *118*, 4027–4038. 10.1242/jcs.02522.

49. Wu, B., Chao, J.A., and Singer, R.H. (2012). Fluorescence Fluctuation Spectroscopy Enables Quantitative Imaging of Single mRNAs in Living Cells. Biophysical Journal *102*, 2936–2944. 10.1016/j.bpj.2012.05.017.

50. Weidinger, G., Stebler, J., Slanchev, K., Dumstrei, K., Wise, C., Lovell-Badge, R., Thisse, C., Thisse, B., and Raz, E. (2003). dead end, a Novel Vertebrate Germ Plasm Component, Is Required for Zebrafish Primordial Germ Cell Migration and Survival. Current Biology *13*, 1429–1434. 10.1016/S0960-9822(03)00537-2.

51. Edelheit, O., Hanukoglu, A., and Hanukoglu, I. (2009). Simple and efficient site-directed mutagenesis using two single-primer reactions in parallel to generate mutants for protein structure-function studies. BMC Biotechnol *9*, 61. 10.1186/1472-6750-9-61.

52. van den Ent, F., and Löwe, J. (2006). RF cloning: A restriction-free method for inserting target genes into plasmids. Journal of Biochemical and Biophysical Methods *67*, 67–74. 10.1016/j.jbbm.2005.12.008.

53. Boldajipour, B., Mahabaleshwar, H., Kardash, E., Reichman-Fried, M., Blaser, H., Minina, S., Wilson, D., Xu, Q., and Raz, E. (2008). Control of Chemokine-Guided Cell Migration by Ligand Sequestration. Cell *132*, 463–473. 10.1016/j.cell.2007.12.034.

54. Wolke, U., Weidinger, G., Köprunner, M., and Raz, E. (2002). Multiple Levels of Posttranscriptional Control Lead to Germ Line-Specific Gene Expression in the Zebrafish. Current Biology *12*, 289–294. 10.1016/S0960-9822(02)00679-6.

55. Westerich, K.J., Chandrasekaran, K.S., Gross-Thebing, T., Kueck, N., Raz, E., and Rentmeister, A. (2020). Bioorthogonal mRNA labeling at the poly(A) tail for imaging localization and dynamics in live zebrafish embryos. Chem. Sci. *11*, 3089–3095. 10.1039/C9SC05981D.

56. Leucht, C., Stigloher, C., Wizenmann, A., Klafke, R., Folchert, A., and Bally-Cuif, L. (2008). MicroRNA-9 directs late organizer activity of the midbrain-hindbrain boundary. Nat Neurosci *11*, 641–648. 10.1038/nn.2115.

57. Katz, S., Cussigh, D., Urbán, N., Blomfield, I., Guillemot, F., Bally-Cuif, L., and Coolen, M. (2016). A Nuclear Role for miR-9 and Argonaute Proteins in Balancing Quiescent and

Activated Neural Stem Cell States. Cell Reports *17*, 1383–1398. 10.1016/j.celrep.2016.09.088.

58. Gross-Thebing, T., Paksa, A., and Raz, E. (2014). Simultaneous high-resolution detection of multiple transcripts combined with localization of proteins in whole-mount embryos. BMC Biol *12*, 55. 10.1186/s12915-014-0055-7.

59. Chan, S.H., Tang, Y., Miao, L., Darwich-Codore, H., Vejnar, C.E., Beaudoin, J.-D., Musaev, D., Fernandez, J.P., Benitez, M.D.J., Bazzini, A.A., et al. (2019). Brd4 and P300 Confer Transcriptional Competency during Zygotic Genome Activation. Developmental Cell *49*, 867-881.e8. 10.1016/j.devcel.2019.05.037.